

Small Molecule Acceptors with a Nonfused Architecture for High-Performance Organic Photovoltaics

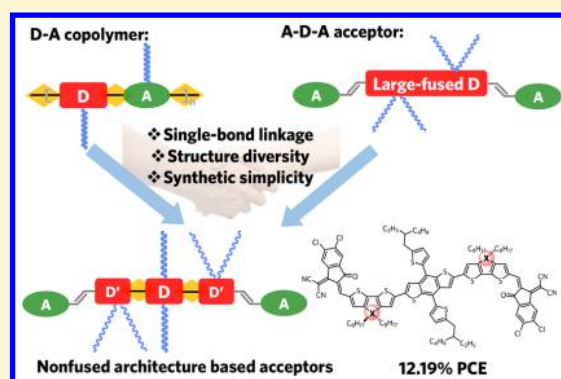
Yuan-Qiu-Qiang Yi,^{†,§} Huanran Feng,^{†,§} Nan Zheng,[‡] Xin Ke,[†] Bin Kan,[†] Meijia Chang,[†] Zengqi Xie,[‡] Xiangjian Wan,[†] Chenxi Li,[†] and Yongsheng Chen^{*,†,§}

[†]The Key Laboratory of Functional Polymer Materials, State Key Laboratory and Institute of Elemento-Organic Chemistry, Centre of Nanoscale Science and Technology, College of Chemistry, Nankai University, Tianjin 300071, China

[‡]Institute of Polymer Optoelectronic Materials and Devices, State Key Laboratory of Luminescent Materials and Devices, South China University of Technology, Guangzhou 510640, China

Supporting Information

ABSTRACT: Different from the widely studied non-fullerene acceptor molecules with a generally large fused backbone architecture, two novel small molecule acceptors (SMAs) with a nonfused architecture, namely, BDTS-4Cl and BDTC-4Cl, have been designed and synthesized with much simpler procedures using dithienosilole (DTS) and cyclopentadithiophene (DTC) as the π donor moieties, respectively. PBDB-T:BDTC-4Cl-based organic solar cells (OSCs) show a power conversion efficiency (PCE) of 9.54% compared to a PCE of 3.73% for PBDB-T:BDTS-4Cl-based OSCs. When using PC₇₁BM as a combinatory acceptor for a ternary system of BDTC-4Cl, the PCE has been enhanced significantly to 12.19%. These results are evidence of the highest-performance OSCs using SMAs with a nonfused framework, comparable to the widely studied large fused SMA-based OSCs. These results indicate that, benefiting from the high diversity of organic molecular structures, further design and studies are urgently needed and also important for exploring and/or optimizing OSC molecules for both better performance and simpler synthesis with different architectures, such as the case presented here with a nonfused architecture.



INTRODUCTION

Recently, non-fullerene small molecule acceptor (NF-SMA)-based organic solar cells (OSCs) have been greatly improved, yielding impressive power conversion efficiencies (PCEs) of >14%.^{1–6} To date, the most successful NF-SMAs usually contain an acceptor–donor–acceptor (A–D–A) backbone structure, which offers a rich platform for manipulating and optimizing the molecule design and morphology and even the optoelectronic process, including the key intramolecular charge transfer (ICT) step.^{7–12} Note that such widely studied A–D–A type NF-SMAs, including ITIC and its analogues, normally employ a large fused central core (D unit) to guarantee backbone planarity, with bulky sp^3 substituents to suppress over-self-aggregation for an ideal morphology.^{8–10} However, such large fused NF-SMAs generally require comparatively long linear synthesis procedures, thus resulting in an overall low yield and high cost.⁷ Also, the sp^3 bulky unit in those systems would simultaneously limit structural diversity. Furthermore, most functional organic and polymeric molecules generally have a donor/acceptor (D/A) alternating structure without a large fused system, which can be synthesized convergently and built by direct coupling reactions using the efficient and easy Stille or Suzuki reaction.^{13,14} More importantly, such a structure and such an easy synthesis offer

much greater structural diversity for the targeted molecules. With these, it is reasonable to believe that there must be other alternatives to the currently widely studied NF-SMAs with a large fused molecular architecture, such as the molecules directly linked by a single bond with various donor and acceptor units without such large fused structures (Figure 1). This would bring not only more diversified building blocks but also synthetic simplicity to the NF-SMA community.

Previously, we reported such a directly linked D/A donor molecule DRDTSBDTT, using 4,8-bis(5-ethylhexyl-2-thienyl)benzo[1,2-*b*:4,5-*b'*]dithiophene (BDTT) as the central core bridged by 4,4'-dioctyl-dithieno[3,2-*b*:2',3'-*d'*]silole (DTS) and end-capped by a rhodanine group.¹⁵ Considering the packing requirements of the morphology for NF-SMAs, generally achieved using a bulky sp^3 carbon between different building units, the DTS unit might fit such a requirement if linked directly with other units. In addition, the two-dimensional sp^2 thiophene unit (BDTT) would simultaneously make some contribution to prevent over-intermolecular aggregation for achieving suitable phase separation domains and purity.^{7,9} In

Received: September 25, 2018

Revised: January 2, 2019

Published: January 4, 2019

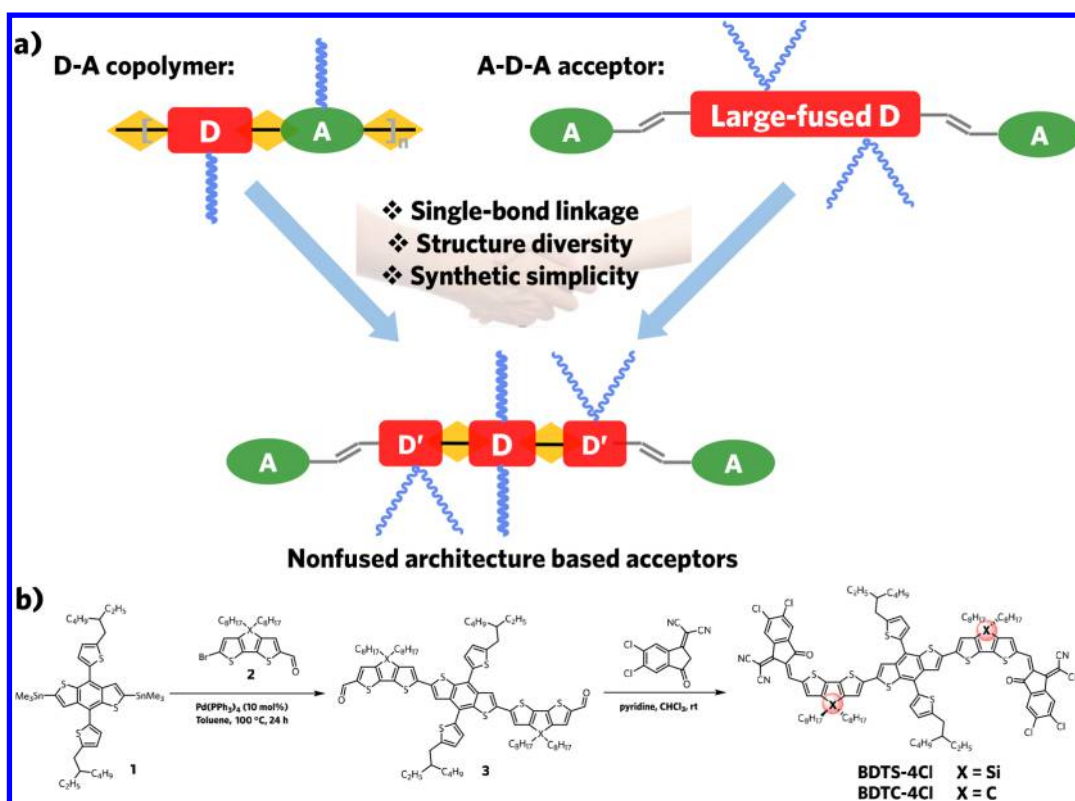


Figure 1. (a) Design strategy for nonfused architecture-based acceptors. (b) Synthetic route.

addition, modifying DRDTSBDTT with a stronger electron-withdrawing ending group would modulate its energy levels for matching with the proper polymer donor. Via combination of these bulky structural features and the suitable frontier energy levels, it thus may be a judicious choice to construct high-performance nonfused architecture-based NF-SMAs from DRDTSBDTT.

On the basis of the considerations described above, two nonfused architecture-based NF-SMAs with a single-bond linkage, namely, BDTS-4Cl and BDTC-4Cl, have been designed and synthesized, originating from our donor DRDTSBDTT.¹⁵ The synthetic route to these two molecules is as simple as only a two-step procedure. BDTS-4Cl and BDTC-4Cl share a similar backbone structure, using BDTT as the central core (D) but employing C- and Si-bridged dithiophenes as their π donor moieties (D'), respectively. A strong electron-withdrawing terminal segment bis(5,6-dichloro-3-oxo-2,3-dihydro-1*H*-indene-2,1-diylidene)-dimalononitrile (IC-2Cl) is used as the end group to downshift highest occupied molecular orbital (HOMO) and lowest unoccupied molecular orbital (LUMO) levels.^{16–19} By pairing with PBDB-T as the polymer donor, the optimal PBDB-T:BDTC-4Cl-based device achieved a much higher PCE of 9.54% compared to that of the PBDB-T:BDTS-4Cl-based device. Furthermore, by using PC₇₁BM as a combinatory acceptor for the BDTC-4Cl-based device, the ternary OSCs realized a significantly enhanced PCE of 12.19%, which is the highest PCE in OSCs based on SMA with a nonfused framework.^{20,21} These results strongly prove that our molecular design strategy with a nonfused architecture linked by a single bond is as effective as a large fused framework for the construction of high-performance SMAs.

■ SYNTHESIS AND THERMAL PROPERTIES

The synthetic route to BDTS-4Cl and BDTC-4Cl is as simple as only a two-step procedure (Stille cross-coupling and Knoevenagel condensation reactions) and depicted in Figure 1b. The detailed synthesis procedures and characterization data are summarized in the Supporting Information. The Stille cross-coupling reaction was performed with commercially available [4,8-bis(5-ethylhexyl-2-thienyl)-benzo[1,2-*b*:4,5-*b'*]-dithiophene-2,6-diyl]bis(trimethylstannane) and 6-bromo-4,4'-dioctyl-dithieno[3,2-*b*:2',3'-*b'*]silole-2-carboxaldehyde or 6-bromo-4,4'-dioctyl-4*H*-cyclopenta[2,1-*b*:3,4-*b'*]dithiophene-2-carboxaldehyde and could generate dialdehyde BDTS-2CHO or BDTC-2CHO, respectively. The target NF-SMAs BDTS-4Cl and BDTC-4Cl were then synthesized by the condensation reaction with IC-2Cl in good yields. BDTS-4Cl and BDTC-4Cl were characterized by nuclear magnetic resonance (NMR) and high-resolution Fourier transform mass spectrometry (HR-FTMS). Because of the six side chains on the two NF-SMAs, they are rather soluble in common organic solvents (dichloromethane, chloroform, and chlorobenzene). The thermal stability of the two molecules was evaluated by thermogravimetric analysis (TGA), as shown in Figure S1. Their decomposition temperatures at 5% weight loss are 341 and 348 °C for BDTS-4Cl and BDTC-4Cl, respectively, indicating they are sufficiently thermally stable for device fabrication.

■ DENSITY FUNCTIONAL THEORY (DFT) CALCULATIONS

In contrast to large fused SMAs such as ITIC and its analogues,^{22–29} BDTS-4Cl and BDTC-4Cl are both based on a simple nonfused framework with only a single-bond linkage. Therefore, DFT (B3LYP/6-31G*) calculations were employed

to evaluate the optimal geometries and energy levels. The optimized geometric structures and the electron-state density distributions in the molecular orbital are shown in Figure 2 and

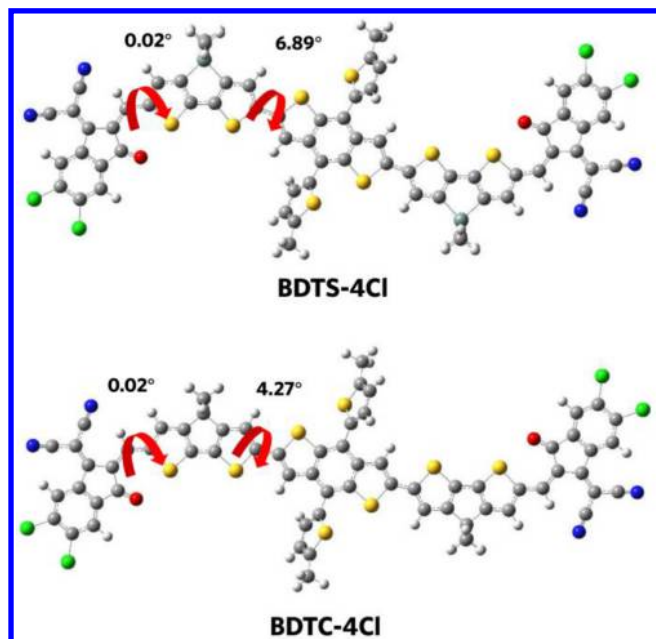


Figure 2. Optimized molecular geometry of BDTS-4Cl and BDTC-4Cl.

Figure S3, indicating an almost planar molecular architecture with dihedral angles of 6.89° and 4.27° between the planar

DTS and DTC and the IC-2Cl combination with the BDTT core, respectively. The calculated HOMO and LUMO energy levels are -5.35 and -3.46 eV for BDTS-4Cl, and -5.37 and -3.48 eV for BDTC-4Cl, respectively.

ELECTROCHEMICAL AND PHOTOPHYSICAL PROPERTIES

The ultraviolet–visible–near-infrared (UV–vis–NIR) absorptions of BDTS-4Cl and BDTC-4Cl were investigated in a dilute solution and in the thin film state (Figure 3). In a dilute chloroform solution, the UV–vis–NIR absorptions of BDTS-4Cl and BDTC-4Cl display similar spectral patterns with maximum absorption peaks at 718 and 737 nm, respectively. From the solution to the solid state, the two molecules exhibit significantly different UV–vis–NIR absorptions. The BDTS-4Cl film shows a broad spectrum with a maximum absorption peak at 680 nm, blue-shifted 38 nm compared with that in solution, but still with an absorption edge up to 850 nm. For the BDTC-4Cl film, a remarkable red-shifted absorption of 68 nm compared to that of its solution state can be observed with the absorption edge up to 873 nm, indicating strong intermolecular π – π stacking. The two acceptor solid films have two more pronounced strong vibration peaks with broader spectra than their solution ones, originating from their strong aggregated state. With regard to the solid aggregate patterns, BDTS-4Cl and BDTC-4Cl exhibit H-aggregate and J-aggregate, respectively.^{30,31} The optical bandgaps (E_g^{opt}) of BDTS-4Cl and BDTC-4Cl can be calculated from the onset of the optical absorption edge of films as 1.46 and 1.42 eV, respectively.

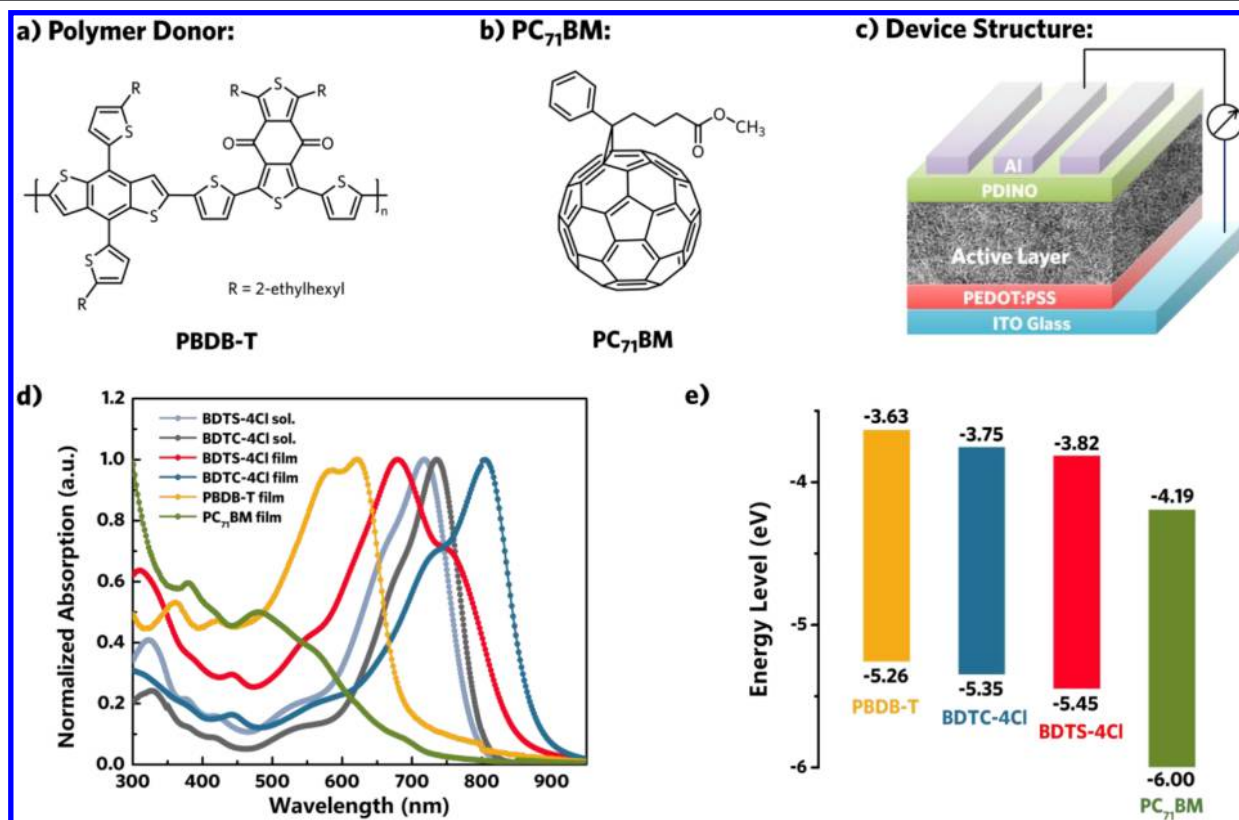


Figure 3. Chemical structures of (a) PBDB-T and (b) PC₇₁BM. (c) Diagram of a conventional device structure. (d) Normalized absorption spectra of BDTS-4Cl, BDTC-4Cl, PBDB-T, and PC₇₁BM. (e) Energy levels of the four compounds.

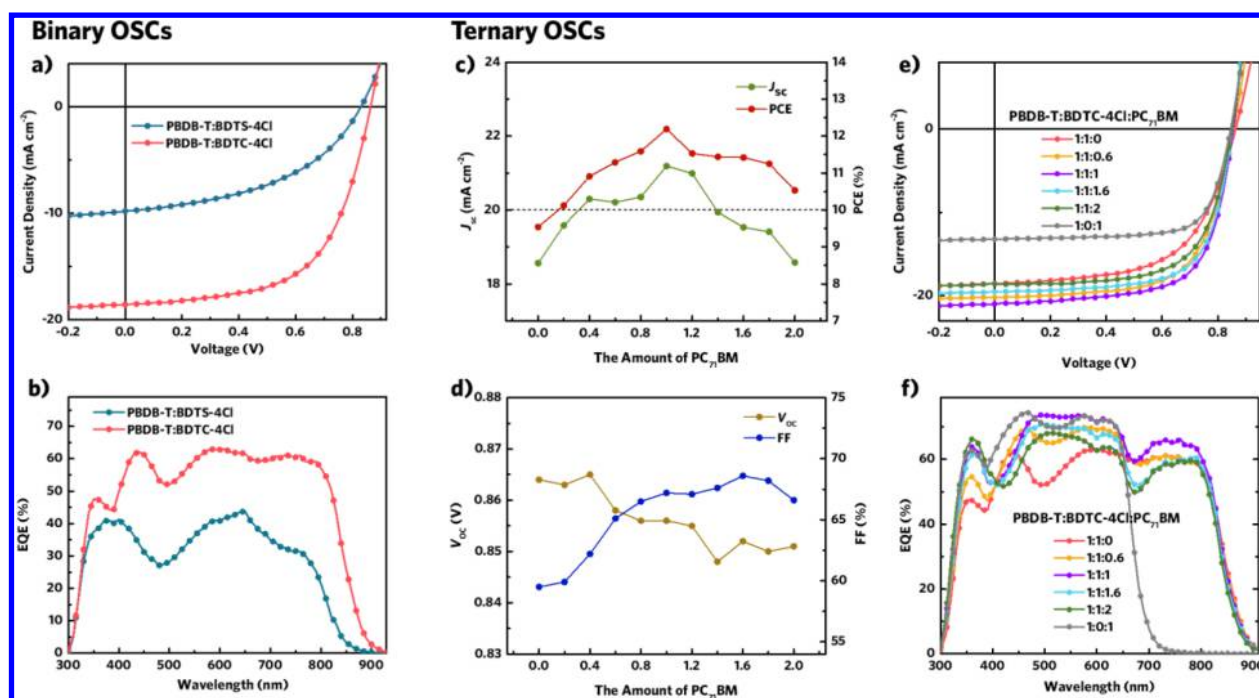


Figure 4. (a) J - V curves and (b) EQE spectra for binary OSCs based on PBDB-T:BDTS-4Cl/BDTC-4Cl. (c) J_{sc} and PCE and (d) V_{oc} and FF vs the amount of PC₇₁BM for ternary OSCs based on PBDB-T:BDTC-4Cl:PC₇₁BM. (e) J - V curves and (f) EQE spectra for ternary devices (with a varied amount of PC₇₁BM).

Table 1. Optimal Device Parameters of the Binary and Ternary Devices under an AM 1.5G Illumination (100 mW cm⁻²) Using the Conventional Device Configuration

active layer ^a	V_{oc} (eV)	J_{sc} (mA cm ⁻²)	FF (%)	PCE ^b (%)
PBDB-T:BDTS-4Cl (1:1)	0.830 (0.828 ± 0.006)	9.80 (9.63 ± 0.50)	45.9 (45.6 ± 0.20)	3.73 (3.58 ± 0.10)
PBDB-T:BDTC-4Cl (1:1)	0.864 (0.865 ± 0.005)	18.56 (17.98 ± 0.60)	59.5 (59.0 ± 0.60)	9.54 (9.42 ± 0.17)
PBDB-T:BDTC-4Cl:PC ₇₁ BM (1:1:1)	0.856 (0.851 ± 0.006)	21.19 (20.71 ± 0.32)	67.2 (66.9 ± 0.40)	12.19 (12.04 ± 0.10)
PBDB-T:PC ₇₁ BM (1:1)	0.847 (0.845 ± 0.003)	13.21 (12.77 ± 0.37)	72.6 (72.5 ± 0.30)	8.12 (7.98 ± 0.24)

^aThe weight ratio of each component. ^bThe average values with standard deviations obtained from 20 devices.

The energy levels of BDTS-4Cl and BDTC-4Cl were determined by electrochemical cyclic voltammetry (Figure S2). The HOMO level and the LUMO level were calculated from the onset oxidation and reduction potentials referenced to ferrocene/ferrocenium (Fc/Fc⁺) (-4.8 eV below the vacuum level) in thin films. The HOMO and LUMO levels are -5.45 and -3.83 eV for BDTS-4Cl and -5.35 and -3.75 eV for BDTC-4Cl, respectively. It is worth noting that the higher LUMO level of BDTC-4Cl may produce a V_{oc} that is higher than that of BDTS-4Cl, which indeed was achieved in devices as presented below.

PHOTOVOLTAIC PROPERTIES

To evaluate the potential photovoltaic performance of BDTS-4Cl and BDTC-4Cl as electron acceptors, solution-processed OSCs were fabricated with a conventional structure of ITO/PEDOT:PSS/PBDB-T:acceptors/PDINO/Al, where PEDOT:PSS and PDINO represent poly(3,4-ethylenedioxythiophene):poly(styrenesulfonate) and perylene diimide functionalized with amino *N*-oxide, respectively. The device achieves a low PCE of 3.73% with a V_{oc} of 0.830 V, a J_{sc} of 9.80 mA cm⁻², and a fill factor (FF) of 45.9%. On the contrary, the PBDB-T:BDTC-4Cl-based device achieves a dramatically higher PCE of 9.54% with a V_{oc} of 0.864 V, a J_{sc} of 18.56 mA cm⁻², and a fill factor (FF) of 59.5%. It is worth

noting that the V_{oc} of 0.864 eV is relatively high considering such a narrow E_g^{opt} of 1.42 eV. The external quantum efficiency (EQE) spectra of the two devices are shown in Figure 4b. Compared with the low and narrow photoresponse from 300 to 850 nm of the PBDB-T:BDTS-4Cl-based device, the PBDB-T:BDTC-4Cl-based device achieves a stronger and broader photoresponse from 300 to ~900 nm and displays a >60% EQE curve from 550 to 800 nm (Table 1).

For the binary PBDB-T:BDTC-4Cl-based device, the moderate EQE and unsatisfactory FF values limit its overall photovoltaic performance. To achieve an ideal fill factor, high and balanced charge carrier mobilities are required. It is known that fullerene and its derivatives usually have much high electron mobilities and great isotropic charge transport properties and have been used as combinatory acceptors to improve photovoltaic performances.³²⁻³⁵ The weight ratio of the binary PBDB-T:BDTC-4Cl-based device was fixed at 1:1, and the amount of PC₇₁BM was comprehensively scanned on a large scale from 0.2 to 3 to acquire an optimal photovoltaic performance for the ternary devices (as depicted in Figure 4e,f and Table S1). The optimal weight ratio was determined to be 1:1:1 for the PBDB-T:BDTC-4Cl:PC₇₁BM-based OSCs, which delivers a significantly enhanced PCE of 12.19% with a nearly 28% promotion. The J_{sc} and FF values of the ternary OSCs increased substantially to 21.19 mA cm⁻² and 67.2%,

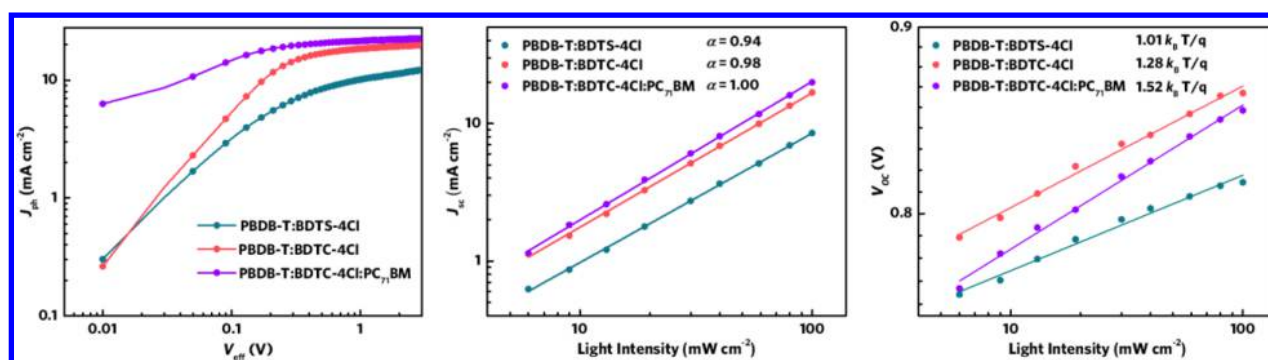


Figure 5. (a) Plot of J_{ph} vs V_{eff} . Correlations between (b) J_{sc} and light intensity and (c) V_{oc} and light intensity in the optimized PBDB-T:BDTS-4Cl-, PBDB-T:BDTC-4Cl-, and PBDB-T:BDTC-4Cl:PC₇₁BM-based devices.

respectively, with an almost unchanged V_{oc} . As displayed in the EQE curves (Figure 4f), this clearly demonstrates that PC₇₁BM could increase the EQE values to >70% in 450–650 nm and >60% in 700–810 nm, which are both much higher than that of the binary control. Besides, as depicted in the IQE curves (Figure S8), the BDTC-4Cl binary and ternary OSCs show average IQE values of 70 and 80%, respectively, in the 350–850 nm region, which are much higher than that of the BDTS-4Cl-based device. This indicates the more efficient charge generation and collection in the BDTC-4Cl-based device. Furthermore, the increased FF value may be ascribed to the ameliorative film morphology and cascade energy levels for more efficient charge transportation and collection.^{36–38} Additionally, there is a trade-off between V_{oc} and FF, but there is a similar variation trend for J_{sc} and PCE (Figure 4c,d). It is worth noting that the ternary device is insensitive to the amount of PC₇₁BM, and a >10% PCE in a large range of 0.2–2 was obtained, which is higher than that of both PBDB-T:PC₇₁BM and PBDB-T:BDTC-4Cl binary OSCs. This insensitivity to the added amount of PC₇₁BM over such a wide range has not been observed before.^{34,37,39,40}

Moreover, the shelf life stabilities of ternary and binary OSCs were both tested. As shown in Figure S7, the BDTC-4Cl-based ternary and binary devices retained 88 and 80%, respectively, of their initial PCE after storage in a glovebox with a N₂ atmosphere in the dark for 15 days, implying that the BDTC-4Cl-based device has a much better stability especially compared to that of its ternary device.

The charge transport properties in the binary and ternary blend films were investigated by the space-charge-limited current (SCLC) method using the electron-only and hole-only devices, respectively. The calculated electron and hole mobilities for PBDB-T:BDTS-4Cl- and PBDB-T:BDTC-4Cl-based devices are 2.61×10^{-4} and 0.83×10^{-4} cm² V⁻¹ s⁻¹ and 1.51×10^{-4} and 1.21×10^{-4} cm² V⁻¹ s⁻¹, respectively. In comparison with a μ_h/μ_e of 3.13 for the BDTS-4Cl-based device, the more balanced μ_h/μ_e of 1.61 of the BDTC-4Cl-based device further explains its much higher J_{sc} and FF.^{41,42} The introduction of PC₇₁BM into BDTC-4Cl binary system produced higher and more balanced electron and hole mobilities ($\mu_h = 2.29 \times 10^{-4}$ cm² V⁻¹ s⁻¹, $\mu_e = 2.06 \times 10^{-4}$ cm² V⁻¹ s⁻¹, and $\mu_h/\mu_e = 1.11$) compared to those of their binary control. The high and balanced charge transport properties of ternary OSCs facilitate efficient charge extraction and collection and suppress bimolecular recombinations, which are partially responsible for their improved FF and J_{sc} and overall elevated performance.^{41,42}

To gain insight into the charge generation and dissociation process in the working devices, the plots of photocurrent density (J_{ph}) versus effective voltage (V_{eff}) were measured. $J_{ph} = J_L - J_D$, where J_L is the current density under illumination and J_D is the current density in the dark. $V_{eff} = V_0 - V_a$, where V_a is the applied voltage and V_0 is the voltage at which J_{ph} is zero.⁴³ As depicted in Figure 5a, when V_{eff} reaches ~ 1.5 V, J_{ph} values for both binary and ternary devices reach saturation (J_{sat}), indicating that charge recombination is minimized at higher voltages due to the high internal electric field in the devices. The exciton dissociation probability [$P(E, T)$] in the working devices could be estimated by calculating the value of J_{ph}/J_{sat} , where E and T represent the field and temperature, respectively.⁴⁴ Under the circumstances of the short circuit and maximal power output, $P(E, T)$ values are 86.8 and 61.3% for the BDTS-4Cl-based device, 94.7 and 73.6% for the BDTC-4Cl-based binary device, and 96.6 and 83.8% for the BDTC-4Cl-based ternary device, respectively. The higher $P(E, T)$ values of BDTC-4Cl-based binary and ternary devices suggest their more efficient exciton dissociation and higher charge transport efficiency compared to those of the BDTS-4Cl-based device, in support of their high FFs.^{43,44}

The light intensity (P_{light}) dependence of J_{sc} was tested to investigate the charge recombination properties of the devices. The relationship between J_{sc} and P can be described by the power law equation $J_{sc} \propto P_{light}^\alpha$, where power law exponent α implies the extent of bimolecular recombination. Weak bimolecular recombination in the device would result in a linear dependence of J_{sc} on light intensity with an α of ~ 1 . As shown in Figure 5b, the α values for the devices based on PBDB-T:BDTS-4Cl, PBDB-T:BDTC-4Cl, and PBDB-T:BDTC-4Cl:PC₇₁BM, are 0.94, 0.98, and 1.00, respectively, indicating that very weak bimolecular recombination occurred in these devices, especially for BDTC-4Cl-based binary and ternary devices.

Furthermore, Figure 5c shows the correlations between V_{oc} and P_{light} in the three devices. The slope of V_{oc} versus P_{light} helps to determine the degree of trap-assisted recombination in the working devices. A slope at $k_B T/q$ implies that the bimolecular recombination mechanism is dominant, where k_B is Boltzmann's constant, T is the temperature, and q is the elementary charge. As for trap-assisted or Shockley–Read–Hall (SRH) recombination, a stronger dependence of V_{oc} on light intensity with a slope of $2 k_B T/q$ is observed. As depicted, the slope for the binary device based on BDTS-4Cl is 1.01 $k_B T/q$, implying that, at the open circuit, bimolecular recombination dominates. The slopes for the BDTC-4Cl-

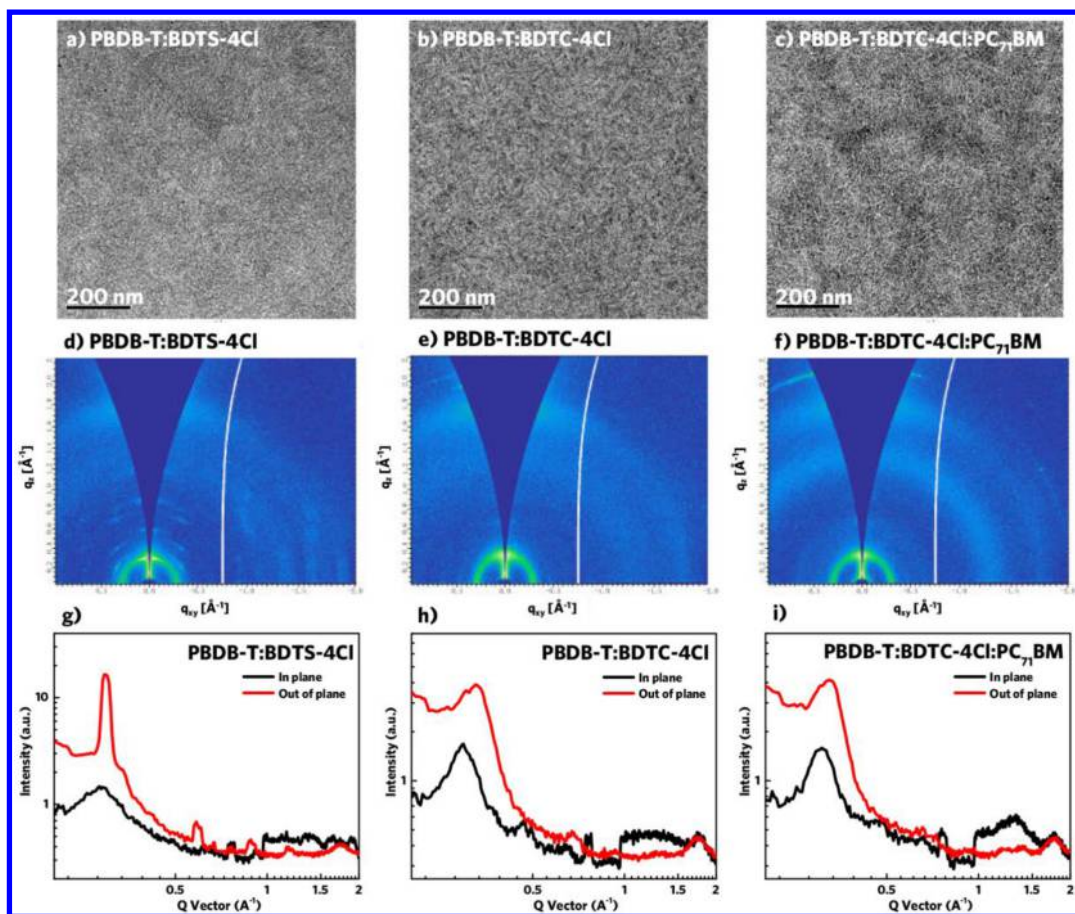


Figure 6. TEM images and GIWAXS patterns of in-plane and out-of-plane line cuts of the corresponding GIWAXS patterns for (a, d, and g) PBDB-T:BDTS-4Cl, (b, e, and h) PBDB-T:BDTC-4Cl, and (c, f, and i) PBDB-T:BDTC-4Cl:PC₇₁BM blend films.

based binary and ternary devices are 1.28 and 1.52 $k_B T/q$, respectively. The stronger dependence of V_{oc} on light intensity implies that recombination at the open circuit in these devices is a combination of monomolecular (SRH) and bimolecular processes.

MORPHOLOGY CHARACTERIZATIONS

To clarify the interfacial and bulk morphology of BDTS-4Cl binary blend and BDTC-4Cl binary/ternary systems, atomic force microscopy (AFM) and transmission electron microscopy (TEM) measurements were taken. As depicted in Figure S5, the three blend films exhibit good miscibility of donors and acceptors with a comparatively small root-mean-square roughness (RMS) of 1.82 nm for PBDB-T:BDTS-4Cl, 1.77 nm for PBDB-T:BDTC-4Cl, and 1.55 nm for PBDB-T:BDTC-4Cl:PC₇₁BM blends. Compared with the BDTS-4Cl-based blend film, the BDTC-4Cl-based one shows a uniform distribution and has fiberlike interpenetrating network nanostructures in the TEM images (Figure 6a–c), suggesting that the donor and acceptor are well mixed with a proper nanoscale morphology. The addition of PC₇₁BM to the PBDB-T:BDTC-4Cl binary blend leads to more defined and continuous interpenetration with a growing grainlike nanostructure.

To further inspect the influence of the crystal or stacking behavior for these two acceptors, grazing incidence wide-angle X-ray scattering (GIWAXS) was performed to characterize the neat films of BDTS-4Cl and BDTC-4Cl. As shown in Figure

S6, the BDTS-4Cl-based pristine film shows a lamellar packing (100) in the out-of-plane (OOP) direction at 0.26 Å⁻¹ and an extremely weak π - π stacking (010) reflection peak, while the neat film of BDTC-4Cl exhibits both an IP lamellar packing (100) peak and a relatively clear OOP π - π stacking (010) peak at 0.32 and 1.78 Å⁻¹, respectively, suggesting that BDTC-4Cl shows a preferred face-on orientation in favor of charge transport.^{45,46}

As shown in Figure 6d–f for the GIWAXS patterns and Figure 6g–i for line-cut profiles, the three blend films all exhibit a lamellar diffraction peak (100) along the IP direction and a π - π stacking diffraction peak (010) in the OOP direction, indicating that the three blends prefer the face-on orientation,^{45–48} and the summary of parameters for the blend films obtained from GIWAXS is presented in Table 2. For binary blends of PBDB-T:BDTS-4Cl and PBDB-T:BDTC-4Cl as depicted in panels d and g of Figure 6 and panels e and h of Figure 6, respectively, the GIWAXS diffractions are mainly dominated by the polymer diffraction signals with (100) diffraction peaks at $q_{xy} = 0.289$ and 0.295 Å⁻¹ and (010) diffraction peaks at $q_z = 1.73$ and 1.74 Å⁻¹, respectively. However, the π - π stacking (010) and lamellar (100) diffraction peaks of PBDB-T:BDTC-4Cl are both more pronounced and sharper than that of PBDB-T:BDTS-4Cl, corresponding to smaller lamellar (d_l) and π - π stacking (d_π) distances of 21.29 and 3.61 Å, respectively, compared to those of BDTS-4Cl (21.74 and 3.63 Å, respectively). This indicated that the BDTC-4Cl-based blend forms stronger molecular

Table 2. Summary of the Parameters for the Blend Films Obtained from GIWAXS

active layer	lamellar (100)	π - π stacking (010)		
	d_1^a (Å) [q_{xy} (Å ⁻¹)]	d_π^b (Å) [q_z (Å ⁻¹)]	fwhm ^c (Å ⁻¹)	CCL ^d (Å)
PBDB-T:BDTS-4Cl	21.74 (0.289)	3.63 (1.73)	0.196	28.53
PBDB-T:BDTC-4Cl	21.29 (0.295)	3.61 (1.74)	0.135	41.42
PBDB-T:BDTC-4Cl:PC ₇₁ BM	20.53 (0.306)	3.55 (1.77)	0.109	51.30

^aThe (100) diffraction peak along the q_{xy} axis. ^bThe (010) diffraction peak along the q_z axis. ^cFull width at half-maximum (fwhm) for the (010) peak along the q_z axis. ^dCoherence length estimated from Scherrer's equation ($CCL = 2\pi k/fwhm$) for the π - π stacking of the face-on crystallite.

packing, which is more suitable for more efficient and balanced charge transport as discussed in SCLC measurements. Upon introduction of PC₇₁BM into the binary PBDB-T:BDTC-4Cl blend, the ternary blend exhibits a shifted (100) peak at 0.306 Å⁻¹ in the IP direction and a broadened (010) peak with a shifted q value of 1.77 Å⁻¹, demonstrating that the addition of PC₇₁BM leads to π - π stacking that is stronger than that in its binary blend. The coherence length (CCL) of the π - π stacking was also found to be increased gradually from 41.42 to 51.30 Å. The privileged morphology of the ternary blend is partly responsible for better charge transport and collection and the resulting better device performance.

CONCLUSIONS

In summary, two SMAs with a nonfused architecture (BDTS-4Cl and BDTC-4Cl) have been designed and synthesized. The synthetic route to the two molecules is much simpler with the nonfused framework linked directly by a single bond. BDTS-4Cl and BDTC-4Cl possess a similar single-bond-linked backbone but use silicon- and carbon-bridged dithiophenes as their π -moieties, respectively. The PBDB-T:BDTC-4Cl-based device gives a PCE of 9.54% that is much higher than the PCE of 3.73% of the BDTS-4Cl-based device. Utilization of PC₇₁BM as a combinatory acceptor enables the BDTC-4Cl binary system to produce an ~28% increase in PCE to 12.19%, which is the highest performance based on SMAs with a nonfused framework and also comparable to that of large fused SMA-based devices. These results indicate, benefiting from the high diversity of organic molecular structures, as a competitive alternative, nonfused architecture-based SMAs can successfully achieve comparable photovoltaic performance with a simpler synthesis. These high-performance results, together with the simpler structure, indicate that there should be much more room to explore and optimize the currently high-performance OPV molecules.

ASSOCIATED CONTENT

Supporting Information

The Supporting Information is available free of charge on the ACS Publications website at DOI: 10.1021/acs.chemmater.8b04087.

Experimental details, characterization data for the new compounds, thermogravimetric analysis, differential scanning calorimetry, cyclic voltammograms, internal quantum efficiencies, J - V characteristics of SCLC, NMR spectra, mass spectra, and other device data (PDF)

AUTHOR INFORMATION

Corresponding Author

*E-mail: yschen99@nankai.edu.cn.

ORCID

Yuan-Qiu-Qiang Yi: 0000-0003-3522-7056

Zengqi Xie: 0000-0002-9805-8176

Yongsheng Chen: 0000-0003-1448-8177

Author Contributions

[§]Y.-Q.-Q.Y. and H.F. contributed equally to this work.

Notes

The authors declare no competing financial interest.

ACKNOWLEDGMENTS

This work was supported by the MoST (2016YFA0200200), NSFC (91633301 and 51773095), Tianjin city (17JCJQC44500 and 17CZDJC31100), and the 111 Project (B12015). This work was supported by the Open Fund of the State Key Laboratory of Luminescent Materials and Devices (South China University of Technology).

REFERENCES

- Zhang, H.; Yao, H.; Hou, J.; Zhu, J.; Zhang, J.; Li, W.; Yu, R.; Gao, B.; Zhang, S.; Hou, J. Over 14% Efficiency in Organic Solar Cells Enabled by Chlorinated Nonfullerene Small-Molecule Acceptors. *Adv. Mater.* **2018**, *30*, 1800613.
- Zhang, S.; Qin, Y.; Zhu, J.; Hou, J. Over 14% Efficiency in Polymer Solar Cells Enabled by a Chlorinated Polymer Donor. *Adv. Mater.* **2018**, *30*, 1800868.
- Xiao, Z.; Jia, X.; Ding, L. Ternary organic solar cells offer 14% power conversion efficiency. *Sci. Bull.* **2017**, *62*, 1562–1564.
- Kan, B.; Feng, H.; Yao, H.; Chang, M.; Wan, X.; Li, C.; Hou, J.; Chen, Y. A chlorinated low-bandgap small-molecule acceptor for organic solar cells with 14.1% efficiency and low energy loss. *Sci. China: Chem.* **2018**, *61*, 1307–1313.
- Zhang, Y.; Yao, H.; Zhang, S.; Qin, Y.; Zhang, J.; Yang, L.; Li, W.; Wei, Z.; Gao, F.; Hou, J. Fluorination vs. chlorination: a case study on high performance organic photovoltaic materials. *Sci. China: Chem.* **2018**, *61*, 1328–1337.
- Wadsworth, A.; Moser, M.; Marks, A.; Little, M. S.; Gasparini, N.; Brabec, C. J.; Baran, D.; McCulloch, I. Critical review of the molecular design progress in non-fullerene electron acceptors towards commercially viable organic solar cells. *Chem. Soc. Rev.* **2019**, DOI: 10.1039/C7CS00892A.
- Zhang, G.; Zhao, J.; Chow, P. C. Y.; Jiang, K.; Zhang, J.; Zhu, Z.; Zhang, J.; Huang, F.; Yan, H. Nonfullerene Acceptor Molecules for Bulk Heterojunction Organic Solar Cells. *Chem. Rev.* **2018**, *118*, 3447–3507.
- Hou, J.; Inganäs, O.; Friend, R. H.; Gao, F. Organic solar cells based on non-fullerene acceptors. *Nat. Mater.* **2018**, *17*, 119–128.
- Cheng, P.; Li, G.; Zhan, X.; Yang, Y. Next-generation organic photovoltaics based on non-fullerene acceptors. *Nat. Photonics* **2018**, *12*, 131–142.
- Yan, C.; Barlow, S.; Wang, Z.; Yan, H.; Jen, A. K. Y.; Marder, S. R.; Zhan, X. Non-fullerene acceptors for organic solar cells. *Nat. Rev. Mater.* **2018**, *3*, 18003.
- Chen, Y.; Wan, X.; Long, G. High performance photovoltaic applications using solution-processed small molecules. *Acc. Chem. Res.* **2013**, *46*, 2645–2655.
- Yang, Y.; Wang, K.; Li, G.; Ran, X.; Song, X.; Gasparini, N.; Zhang, Q. Q.; Lai, X.; Guo, X.; Meng, F.; Du, M.; Huang, W.; Baran, D. Fluorination Triggered New Small Molecule Donor Materials for Efficient As-Cast Organic Solar Cells. *Small* **2018**, *14*, 1801542.
- Cai, Y.; Huo, L.; Sun, Y. Recent Advances in Wide-Bandgap Photovoltaic Polymers. *Adv. Mater.* **2017**, *29*, 1605437.

- (14) Yao, H.; Ye, L.; Zhang, H.; Li, S.; Zhang, S.; Hou, J. Molecular Design of Benzodithiophene-Based Organic Photovoltaic Materials. *Chem. Rev.* **2016**, *116*, 7397–7457.
- (15) Yi, Z.; Ni, W.; Zhang, Q.; Li, M.; Kan, B.; Wan, X.; Chen, Y. Effect of thermal annealing on active layer morphology and performance for small molecule bulk heterojunction organic solar cells. *J. Mater. Chem. C* **2014**, *2*, 7247–7255.
- (16) Cui, Y.; Yang, C.; Yao, H.; Zhu, J.; Wang, Y.; Jia, G.; Gao, F.; Hou, J. Efficient Semitransparent Organic Solar Cells with Tunable Color enabled by an Ultralow-Bandgap Nonfullerene Acceptor. *Adv. Mater.* **2017**, *29*, 1703080.
- (17) Li, Y.; Lin, J. D.; Che, X.; Qu, Y.; Liu, F.; Liao, L. S.; Forrest, S. R. High Efficiency Near-Infrared and Semitransparent Non-Fullerene Acceptor Organic Photovoltaic Cells. *J. Am. Chem. Soc.* **2017**, *139*, 17114–17119.
- (18) Tang, M. L.; Oh, J. H.; Reichardt, A. D.; Bao, Z. Chlorination: a general route toward electron transport in organic semiconductors. *J. Am. Chem. Soc.* **2009**, *131*, 3733–3740.
- (19) Fan, Q.; Zhu, Q.; Xu, Z.; Su, W.; Chen, J.; Wu, J.; Guo, X.; Ma, W.; Zhang, M.; Li, Y. Chlorine substituted 2D-conjugated polymer for high-performance polymer solar cells with 13.1% efficiency via toluene processing. *Nano Energy* **2018**, *48*, 413–420.
- (20) Li, S.; Zhan, L.; Liu, F.; Ren, J.; Shi, M.; Li, C. Z.; Russell, T. P.; Chen, H. An Unfused-Core-Based Nonfullerene Acceptor Enables High-Efficiency Organic Solar Cells with Excellent Morphological Stability at High Temperatures. *Adv. Mater.* **2018**, *30*, 1705208.
- (21) Zhan, L.; Li, S.; Zhang, H.; Gao, F.; Lau, T. K.; Lu, X.; Sun, D.; Wang, P.; Shi, M.; Li, C. Z.; Chen, H. A Near-Infrared Photoactive Morphology Modifier Leads to Significant Current Improvement and Energy Loss Mitigation for Ternary Organic Solar Cells. *Adv. Mater.* **2018**, *5*, 1800755.
- (22) Yi, Y.-Q.-Q.; Feng, H.; Chang, M.; Zhang, H.; Wan, X.; Li, C.; Chen, Y. New small-molecule acceptors based on hexacyclic naphthalene(cyclopentadithiophene) for efficient non-fullerene organic solar cells. *J. Mater. Chem. A* **2017**, *5*, 17204–17210.
- (23) Lin, Y.; Wang, J.; Zhang, Z. G.; Bai, H.; Li, Y.; Zhu, D.; Zhan, X. An electron acceptor challenging fullerenes for efficient polymer solar cells. *Adv. Mater.* **2015**, *27*, 1170–1174.
- (24) Lin, Y.; Zhang, Z.-G.; Bai, H.; Wang, J.; Yao, Y.; Li, Y.; Zhu, D.; Zhan, X. High-performance fullerene-free polymer solar cells with 6.31% efficiency. *Energy Environ. Sci.* **2015**, *8*, 610–616.
- (25) Kan, B.; Feng, H.; Wan, X.; Liu, F.; Ke, X.; Wang, Y.; Zhang, H.; Li, C.; Hou, J.; Chen, Y. Small-Molecule Acceptor Based on the Heptacyclic Benzodi(cyclopentadithiophene) Unit for Highly Efficient Nonfullerene Organic Solar Cells. *J. Am. Chem. Soc.* **2017**, *139*, 4929–4934.
- (26) Qiu, N.; Zhang, H.; Wan, X.; Li, C.; Ke, X.; Feng, H.; Kan, B.; Zhang, H.; Zhang, Q.; Lu, Y.; Chen, Y. A New Nonfullerene Electron Acceptor with a Ladder Type Backbone for High-Performance Organic Solar Cells. *Adv. Mater.* **2017**, *29*, 1604964.
- (27) Dai, S.; Li, T.; Wang, W.; Xiao, Y.; Lau, T. K.; Li, Z.; Liu, K.; Lu, X.; Zhan, X. Enhancing the Performance of Polymer Solar Cells via Core Engineering of NIR-Absorbing Electron Acceptors. *Adv. Mater.* **2018**, *30*, 1706571.
- (28) Zhu, J.; Ke, Z.; Zhang, Q.; Wang, J.; Dai, S.; Wu, Y.; Xu, Y.; Lin, Y.; Ma, W.; You, W.; Zhan, X. Naphthodithiophene-Based Nonfullerene Acceptor for High-Performance Organic Photovoltaics: Effect of Extended Conjugation. *Adv. Mater.* **2018**, *30*, 1704713.
- (29) Liu, W.; Zhang, J.; Zhou, Z.; Zhang, D.; Zhang, Y.; Xu, S.; Zhu, X. Design of a New Fused-Ring Electron Acceptor with Excellent Compatibility to Wide-Bandgap Polymer Donors for High-Performance Organic Photovoltaics. *Adv. Mater.* **2018**, *30*, 1800403.
- (30) Spano, F. C. The spectral signatures of Frenkel polarons in H- and J-aggregates. *Acc. Chem. Res.* **2010**, *43*, 429–439.
- (31) Mas-Montoya, M.; Janssen, R. A. J. The Effect of H- and J-Aggregation on the Photophysical and Photovoltaic Properties of Small Thiophene-Pyridine-DPP Molecules for Bulk-Heterojunction Solar Cells. *Adv. Funct. Mater.* **2017**, *27*, 1605779.
- (32) Lu, L.; Zheng, T.; Wu, Q.; Schneider, A. M.; Zhao, D.; Yu, L. Recent Advances in Bulk Heterojunction Polymer Solar Cells. *Chem. Rev.* **2015**, *115*, 12666–12731.
- (33) Guldi, D. M.; Illescas, B. M.; Atienza, C. M.; Wielopolski, M.; Martin, N. Fullerene for organic electronics. *Chem. Soc. Rev.* **2009**, *38*, 1587–1597.
- (34) Lu, H.; Zhang, J.; Chen, J.; Liu, Q.; Gong, X.; Feng, S.; Xu, X.; Ma, W.; Bo, Z. Ternary-Blend Polymer Solar Cells Combining Fullerene and Nonfullerene Acceptors to Synergistically Boost the Photovoltaic Performance. *Adv. Mater.* **2016**, *28*, 9559–9566.
- (35) Gao, H. H.; Sun, Y.; Wan, X.; Ke, X.; Feng, H.; Kan, B.; Wang, Y.; Zhang, Y.; Li, C.; Chen, Y. A New Nonfullerene Acceptor with Near Infrared Absorption for High Performance Ternary-Blend Organic Solar Cells with Efficiency over 13. *Adv. Mater.* **2018**, *5*, 1800307.
- (36) Baran, D.; Ashraf, R. S.; Hanifi, D. A.; Abdelsamie, M.; Gasparini, N.; Rohr, J. A.; Holliday, S.; Wadsworth, A.; Lockett, S.; Neophytou, M.; Emmott, C. J.; Nelson, J.; Brabec, C. J.; Amassian, A.; Salleo, A.; Kirchartz, T.; Durrant, J. R.; McCulloch, I. Reducing the efficiency-stability-cost gap of organic photovoltaics with highly efficient and stable small molecule acceptor ternary solar cells. *Nat. Mater.* **2017**, *16*, 363–369.
- (37) Lu, L.; Kelly, M. A.; You, W.; Yu, L. Status and prospects for ternary organic photovoltaics. *Nat. Photonics* **2015**, *9*, 491–500.
- (38) Gasparini, N.; Jiao, X.; Heumueller, T.; Baran, D.; Matt, G. J.; Fladischer, S.; Spiecker, E.; Ade, H.; Brabec, C. J.; Ameri, T. Designing ternary blend bulk heterojunction solar cells with reduced carrier recombination and a fill factor of 77%. *Nat. Energy* **2016**, *1*, 16118.
- (39) Yu, R.; Yao, H.; Hou, J. Recent Progress in Ternary Organic Solar Cells Based on Nonfullerene Acceptors. *Adv. Energy Mater.* **2018**, *8*, 1702814.
- (40) Liu, X.; Yan, Y.; Yao, Y.; Liang, Z. Ternary Blend Strategy for Achieving High-Efficiency Organic Solar Cells with Nonfullerene Acceptors Involved. *Adv. Funct. Mater.* **2018**, *28*, 1802004.
- (41) Proctor, C. M.; Love, J. A.; Nguyen, T. Q. Mobility guidelines for high fill factor solution-processed small molecule solar cells. *Adv. Mater.* **2014**, *26*, 5957–5961.
- (42) Bartesaghi, D.; Pérez, I. d. C.; Kniepert, J.; Roland, S.; Turbiez, M.; Neher, D.; Koster, L. J. Competition between recombination and extraction of free charges determines the fill factor of organic solar cells. *Nat. Commun.* **2015**, *6*, 7083.
- (43) Blom, P. W. M.; Mihailetschi, V. D.; Koster, L. J. A.; Markov, D. E. Device physics of polymer: fullerene bulk heterojunction solar cells. *Adv. Mater.* **2007**, *19*, 1551–1566.
- (44) Proctor, C. M.; Kuik, M.; Nguyen, T. Q. Charge carrier recombination in organic solar cells. *Prog. Polym. Sci.* **2013**, *38*, 1941–1960.
- (45) Mukherjee, S.; Proctor, C. M.; Tumbleston, J. R.; Bazan, G. C.; Nguyen, T. Q.; Ade, H. Importance of domain purity and molecular packing in efficient solution-processed small-molecule solar cells. *Adv. Mater.* **2015**, *27*, 1105–1111.
- (46) Liu, F.; Gu, Y.; Shen, X.; Ferdous, S.; Wang, H.-W.; Russell, T. P. Characterization of the morphology of solution-processed bulk heterojunction organic photovoltaics. *Prog. Polym. Sci.* **2013**, *38*, 1990–2052.
- (47) Muller-Buschbaum, P. The active layer morphology of organic solar cells probed with grazing incidence scattering techniques. *Adv. Mater.* **2014**, *26*, 7692–7709.
- (48) Li, W.; Albrecht, S.; Yang, L.; Roland, S.; Tumbleston, J. R.; McAfee, T.; Yan, L.; Kelly, M. A.; Ade, H.; Neher, D.; You, W. Mobility-controlled performance of thick solar cells based on fluorinated copolymers. *J. Am. Chem. Soc.* **2014**, *136*, 15566–15576.